Cancer Letters 461 (2019) 78–89

Contents lists available at ScienceDirect

Cancer Letters

journal homepage: www.elsevier.com/locate/canlet

Original Articles

Higd-1a regulates the proliferation of pancreatic cancer cells through a pERK/p27^{KIP1}/pRB pathway

Hyun-Jung An[a,1], Mihyeun Ryu[b,1], Hye Jin Jeong[c], Minho Kang[d], Hyung-Min Jeon[c], Jie-Oh Lee[c], Young Sang Kim[b,**], Hayyoung Lee[e,*]

[a] Integrated Research Institute of Pharmaceutical Sciences, BRL & BK21 Plus Team, Pharmaceutical Biochemistry, College of Pharmacy, The Catholic University of Korea, Bucheon, 14662, Gyeonggi-do, Republic of Korea
[b] Department of Biochemistry, College of Natural Science, Chungnam National University, Daejeon, 34134, Republic of Korea
[c] Department of Life Sciences, Pohang University of Science and Technology (POSTECH), Pohang, 37673, Kyeongsangbuk-do, Republic of Korea
[d] Personalized Genomic Medicine Research Center, Korea Research Institute of Bioscience and Biotechnology, Daejeon, 34141, Republic of Korea
[e] Institute of Biotechnology, Chungnam National University, Daejeon, 34134, Republic of Korea

ARTICLE INFO

Keywords:
HIMP1-a
HIG1
Oncogene
Cell cycle
Senescence

ABSTRACT

Higd-1a/HIMP1-a/HIG1, a mitochondrial inner membrane protein, promotes cell survival under low glucose and hypoxic conditions. We previously reported that it interacts with Opa1, a factor involved in mitochondrial fusion, to regulate mitochondrial homeostasis. In the present study, we found that depletion of Higd-1a inhibited the proliferation of pancreatic cancer cells *in vitro* and in mice xenografts. Higd-1a knockdown did not itself lead to cell death but it caused cell cycle arrest through induction of p27^{KIP1} and hypo-phosphorylation of RB protein. Knockdown of Higd-1a also induced cellular senescence as shown by increased granularity and SA-β-galactosidase activity. We further showed that the mitochondrial stress induced by Higd-1a led to reduced ERK phosphorylation. Inhibition of the ERK pathway with U0126 induced p27^{KIP1} expression in the pancreatic cancer cells, confirming that the cell cycle retardation was the result of inhibition of the ERK pathway. Array analysis of human pancreatic cancers revealed that expression of Higd-1a was significantly elevated in pancreatic cancer tissues compared to normal tissue. Collectively, our results demonstrate that Higd-1a plays an important role in the proliferation of pancreatic cancer cells by regulating the pERK/p27^{KIP1}/pRB signaling pathway.

1. Introduction

Mitochondria are active organelles involved in important intracellular functions, including energy production, calcium and redox homeostasis, apoptosis and the supply of building blocks for new cells [1–3]. The observation that cancers carry out aerobic glycolysis by fermenting glucose to lactate in the presence of oxygen was the basis of an earlier proposal that mitochondrial respiration is defective in cancers. However, in most cancers the respiratory function of mitochondria is intact. Furthermore, there is evidence that mitochondrial activity is required for cancer cell proliferation. Thus, impaired mitochondrial function due to loss of the mitochondrial transcription factor A (TFAM) gene delayed the growth of the KRAS-driven lung tumor [4]. When mitochondrial DNA was deleted in B16 melanoma and 4T1 breast carcinoma cells by inhibiting mtDNA replication, tumor growth was reduced [5]. Tumors reprogram anabolic and metabolic pathways to promote their own growth. During the reprogramming of cancer cells, mitochondrial oxidative phosphorylation plays important roles in supplying intermediates and maintaining redox balance as well as in generating energy [6].

Mitochondrial homeostasis is maintained by the combined effects of nuclear and cytoplasmic signaling and the mitochondria themselves [7]. Mitochondrial biogenesis is stimulated by information provided to the nucleus by the cytoplasm and intracellular organelles, and damaged mitochondria are scavenged by mitophagic processes. Mitochondria are highly dynamic organelles subject to continuous fusion and fission that are essential for maintaining their morphology and activity. OPA1, MFN1/2, DRP1 and Fis are key proteins involved in mitochondrial fusion and fission [8–12].

Higd-1a (hypoxia-induced gene domain protein-1a) was previously

* Corresponding author.
** Corresponding author.
E-mail addresses: young@cnu.ac.kr (Y.S. Kim), hlee@cnu.ac.kr (H. Lee).
[1] contributed equally to this work.

https://doi.org/10.1016/j.canlet.2019.07.007
Received 24 January 2019; Received in revised form 24 June 2019; Accepted 11 July 2019

referred to as HIMP1-a (hypoglycemia/hypoxia inducible mitochondrial protein1-a) [13] or just HIG1 [14]. It is a 10.4kDa mitochondrial inner membrane protein, predicted to have two transmembrane domains oriented in an "N-terminal outside-C-terminal outside and loop inside" conformation [13]. It is induced by hypoxia and hypoglycemia [13–16]. Ectopic expression of Higd-1a promoted the survival of pancreatic β cells under stress conditions *in vitro* and in transgenic mice [13,15]. We also reported that Higd-1a-overexpressing macrophages underwent significantly less apoptosis because release of cytochrome *c* was inhibited and they had reduced caspase activities [16]. Higd-1a has been shown to be an interactor of OPA1, to inhibit mitochondrial γ-secretase, and to interact with complexes in the electron transport chain [17–20]. Although further research is required to confirm the effects of Higd-1a interactions with these proteins, it is clear that Higd-1a is a positive regulator of mitochondrial homeostasis and plays a role in cell survival. In the present study, we examined the effect of Higd-1a on pancreatic cancer cell growth and the downstream effects of its depletion. Our aim was to understand the connection between the disruption of mitochondrial function by depleting Higd-1a and inhibition of malignant cancer cell growth.

2. Materials and methods

2.1. Antibodies and reagents

Anti-p-ERK1/2 (#4376), anti-ERK1/2 (#4695), anti-p-p38MAPK (#9215), anti-p38MAPK (#9212), anti-p-AKT (Ser473) (#4060), anti-AKT (#4685) and anti-$p27^{KIP1}$ (#2552), anti-p-mTor (Ser2448 #2971), anti-p-mTor (Ser2481 #2974), anti-mTor (#2983), anti-p-p70S6K (#2905), anti-p70S6K (#2708), anti-p-SAPK/JNK (#9251), anti-SAPK/JNK (#9258), anti-p-AMPK (#4188), anti-AMPK (#2532) and β-actin were purchased from Cell Signaling Technology (Danvers, MA). Antibody against Cyclin D1 (ab134175) were from Abcam (Cambridge, UK). Anti-Cyclin E (sc-481), anti-GSK-3β (sc-9166), anti-BrdU, goat anti-rabbit IgG-HRP (sc-2004) and goat anti-mouse IgG-HRP (sc-2005) were from Santa Cruz Biotechnology (Dallas, TX). Anti-α-tubulin (T6074) and anti-flag-HRP (A8592) were from Sigma-Aldrich (St. Louis, MO). Anti-RB (554136) was from BD Biosciences Pharmingen (San Jose, CA). Chemical inhibitors of MEK (U0126) and p38MAPK (SB203580) were purchased from Calbiochem (San Diego, CA). Trypan blue were from Life Technologies (Carlsbad, CA). Rabbit anti-Higd-1a antibody was raised against a synthetic peptide corresponding to residues 9–21 of human Higd-1a and further purified by affinity chromatography before use. N-terminal Flag-tagged Higd-1a was prepared by cloning into pBICEP-CMV-2 (Sigma Aldrich).

2.2. Cell culture

PANC-1 human pancreatic carcinoma cells and AsPC-1 human pancreatic adenocarcinoma cells were obtained from the Korean Cell Line Bank (Seoul, Korea). PANC-1 cells were cultured in DMEM (Welgene, Gyeongsan, Korea) supplemented with 10% (v/v) heat inactivated fetal bovine serum (FBS) (Hyclone, South Logan, UT) and 1x antibiotic-antimycotic (Gibco-BRL, Waltham, MA). AsPC-1 cells were cultured in RPMI medium (Welgene) supplemented with 10% (v/v) FBS and 1x antibiotic-antimycotic. Cells were grown at 37 °C in a humidified atmosphere with 5% CO_2.

2.3. RT-PCR

Total RNA was isolated with Trizol (Invitrogen) and reverse transcribed with M-MLV Reverse Transcriptase (Promega, Madison, WI). Semi-quantitative RT-PCR was performed with pairs of specific primers, as shown in Tables S1 and S2.

2.4. Immunoblotting

Cultured cells were lysed in RIPA lysis buffer (EMD Millipore, Billerica, MA) with protease inhibitors (Sigma-Aldrich) and phosphatase inhibitors (phosSTOP; Sigma-Aldrich). The lysates were incubated on ice for 20min and supernatants were collected by centrifugation. Samples of 10–30 μg protein were resolved by SDS-PAGE and transferred to a polyvinylidene difluoride membranes (GE Healthcare, Chicago, IL) in a Semi-Dry Blotter (ATTO, Tokyo, Japan). After blocking in PBS with 0.05% Tween 20 plus 5% non-fat dried milk for 1 h at room temperature, membranes were stained with suitable primary antibody at 4 °C overnight and secondary antibody at room temperature for 1 h. The membranes were processed with EzCapture II (ATTO). For Higd-1a-Flag reconstitution, cells were transfected with the Higd-1a-Flag plasmid using the Lipofectamine 2000 transfection reagent (Invitrogen).

2.5. shRNA lentiviral preparation and infection, and siRNA transfection

pLKO.1-puro shRNA plasmid DNAs for human Higd-1a and control were purchased from Sigma-Aldrich. The sequences are; A TRCN0000121999: CCGGGCATTGTTGCATATG GATTACTCGAGTAAT CCATATGCAACAATTGCTTTTTTG; B TRCN0000122388: CCGGGC CCAAGGCTTTGTTGTAGGACTCGAGTCCTACAACAAAGCCTTGGGCTT TTTTG; C TRCN 0000142458: CGGGCTAAAGAGGCACCATTCGTACTC GAGTACGAATGGTGCCTCTTTAG CTTTTTTG; D TRCN0000143367: CCGGGCTATTCCATGTATCGGGAATCTCGAGATTCCC GATACATGGAA TAGCTTTTTTG; E TRCN0000143716: CCGGGTTGTAGGAGCAATGA CTG TTCTCGAGAACAGTCATTGCTCCTACAACTTTTTTG and control: CCGGGTTGTA GGAGCAATGACTGTTCTCGAGAACAGTCATTGCTCCTA CAACTTTTTTG. To produce the lentivirus, HEK293T cells were transfected with 4 μg pLKO.1-puro shRNA plasmid DNA, 4 μg psPAX2 (Addgene, Cambridge, MA) and 2 μg pMDG (Addgene) using X-tremeGENE HP DNA transfection reagent (Roche, Basel, Switzerland). After 72 h, the cell cultures were centrifuged, and the supernatants were filter-sterilized and stored at −72 °C. To decide on the appropriate titer of virus, cells were infected with serially diluted viral supernatants plus 8 μg/ml polybrene (Sigma-Aldrich) for 6–16 h and fresh culture medium was substituted. After 72 h, cells were selected with 1 μg/ml puromycin (Sigma-Aldrich) for 48 h. Higd-1a expression levels were determined by immunoblotting.

siRNA-mediated knockdown was performed using specific siRNA and scrambled siRNA as negative control (Bioneer, Daejeon, Korea). The siRNA sequences were 5′-CCU ACG CCA CCA AUU UCG U-3′ as negative control, 5′-GAC CGA AUU ACU AGU GAC U-3′ for Higd-1a and 5′-CGA CGA UUC UUC UAC UCA A-3′ for $p27^{KIP1}$. Cells were transfected with 10 nM of each siRNA using the Lipofectamine RNAiMAX reagent (Invitrogen).

2.6. Tumor xenografts

Six-week-old female nude mice were obtained from Daehan Biolink (Eumseong, Korea). All animal procedures were approved and guided by the Institutional Animal Care and Use Committee (IACUC) of Chungnam National University (CNU-01055). Mice were injected subcutaneously on the left or right side of the back with 1×10^6 human cancer cells infected with a control or Higd-1a shRNA in 200 μl PBS including 35% matrigel (BD Bioscience, San Jose, CA). When the resulting tumors became visible with the naked eye, they were measured every 3 days using a caliper, and tunor volumes (cm^3) were calculated as (length) x (width) x (height)/2. After the mice were killed, the tumors were removed and weighed. They were immediately frozen in liquid nitrogen for further analysis by immunoblotting.

2.7. Senescence β-galactosidase staining

Cells were seeded in 6-well plates at 1.5×10^5 per well. SA-β-gal staining was performed with a Senescence Cells Histochemical Staining Kit (Sigma, St. Louis, MO), following the manufacturer's protocol.

2.8. Assessment of cell growth

For the MTT assay, 50 μl of 1 mg/ml MTT (3-(4,5-dimthylthiazol-2-yl)-2,5-diphenyltetrazolium bromide), (Duchefa Niochemie, Haarlem, Netherlands) was included in each plate for the last 4 h of incubation. The formazan produced by viable cells was dissolved in dimethyl sulfoxide and absorbance was measured at 540 nm.

2.9. Flow cytometric analysis

For cell cycle analysis, 1×10^6 cells were fixed by dropwise addition to 70% ice-cold ethanol and incubated overnight at 4 °C. The cells were pelleted and resuspended in 0.2 ml PBS containing 50 μg/ml of propidium iodide (Molecular PI, Probes) and 0.1 μg/ml of RNase A (Sigma-Aldrich). After at least 30 min at room temperature, the cells were acquired with a FACSCalibur flow cytometer using CELLQuest (BD Biosciences). Data were analyzed with ModFit LT Version 3.0 software. Annexin V binding and PI staining of apoptotic cells were performed with a FITC Annexin V Apoptosis Detection Kit II (BD Biosciences), following the manufacturer's instructions. To measure cell size and granularity, 1×10^5 cells were analyzed by forward scatter and side scatter measurements, respectively.

2.10. NF-κB reporter assays

Control- and shRNA-infected cells were transfected with a reporter plasmid driven by NF-κB promoter and pRL-TK, an internal control plasmid expressing the *Renilla* luciferase gene (Promega) after 5 days of infection. Transfections were performed using X-tremeGENE HP DNA transfection reagent (Roche). After 48 h, *Firefly* and *Renilla* luciferase activities were measured sequentially in cell lysates using a Dual-Luciferase reporter assay system (Promega) with a VICTOR^3 multi-label reader (Perkin Elmer, Waltham, MA).

2.11. NADH redox status

Cells were infected with lentivirus expressing control or Higd-1a shRNA. After 3–7 days of infection, the NAD+/NADH ratio was measured using a NAD+/NADH Glo Assay kit (Promega). Luminescence was read on a VICTOR^3 multi-label reader (Perkin Elmer).

2.12. Human gene expression omnibus (GEO) data

Human gene expression data were acquired from the National Center for Biotechnology Information (NCBI) GEO database (http://www.ncbi.nlm.nih.gov/geo/), under accession numbers GDS4102 and GDS4336. The GDS4102 datasets consist of human pancreatic gene expression data from tissues of patients, with 36 tumor samples and 16 normal samples. The GDS4336 datasets consist of human pancreatic gene expression data from tissues of patients with pancreatic ductal adenocarcinoma tumors (n = 45) and adjacent non-tumor tissue (n = 45). The association between Higd-1a expression and expression of cell cycle regulator genes was evaluated by Pearson's correlation coefficient.

2.13. Immunohistochemistry

Human pancreatic tissue specimens (paired normal and cancer tissues from each patient, $n = 12$) were obtained from the Daegu Dongsan Hospital Biobank (Keimyung University, Daegu, Korea). The ethics committee at our institution approved the use of the tissue specimens for research (201902-BR-019-01). Immunohistochemistry was performed using DAKO Envision Polymer kits. Briefly, formalin-fixed, paraffin-embedded tissue sections 3 μM thick were deparaffinized and rehydrated. Heat-induced epitope retrieval was performed using a citrate buffer (pH 6.0) in a steamer set (IHC world, Ellicott City, Maryland) at 120v, 60Hz, 650w for 45 min. The endogenous peroxidase activity was blocked using 3% H_2O_2 in methanol for 10 min. Tissue sections were then incubated for 60 min with 1/100 of rabbit monoclonal anti-Ki-67 (Cell Marque, Rocklin, CA) or anti-Higd-1a antibodies at 25 °C in a humidified chamber. After washing three times for 5 min with TBS, tissue slides were incubated with EnVision + System-HRP Labelled Polymer anti-Rabbit as per the manufacturer's instructions (Dako, Santa Clara, CA). Tissue sections were incubated with 3,3′-diaminobenzidine/H_2O_2 for color development and counter-stained with mayer's hematoxylin (Dako). The stained tissue slides were dehydrated and mounted in a synthetic mountant (Thermo Scientific, Waltham, MA). To obtain histomorphometric measurements, each specimen was photographed in three different fields randomly selected with an OLYMPUS BX53 microscope (Olympus, Tokyo, Japan) using a DP70 microscopic digital camera. The Higd-1a expression levels were measured with ImageJ software. The mean score for each patient was then determined by summing all scores. The number of Ki-67-positive cells was determined by manual counting in 20 random visual fields.

2.14. Statistical analyses

Data are presented as means ± standard errors (S.E.) of at least three independent experiments. Statistical significance was analyzed with GraphPad Prism software version 5.01 for Windows (GraphPad Software, San Diego, CA). Individual comparisons were made using two-tailed Student t-tests and two-way Anova multiple comparisons. p values of < 0.05 were considered significant.

3. Results

3.1. Silencing of Higd-1a slows the growth of cancer cells

First, we sought to identify the cellular changes resulting from Higd-1a silencing in AsPC-1 and PANC-1 pancreatic adenocarcinoma cells. The Higd-1a protein was reduced by 80–90% in these cell lines, which were tested for up to 6 days after transfection with siRNA (Fig. 1A), and this Higd-1a silencing led to growth inhibition of both cell lines, as defined by trypan blue exclusion. After 6 days, cell numbers in the Higd-1a-depleted AsPC-1 and PANC-1 cultures were only 30 and 47%, respectively, of those in control siRNA-transfected cells (Fig. 1B). Lentiviral shRNA against Higd-1a were also tested. Five different lentiviral shRNA were tested, and most of clones were found to efficiently knockdown Higd-1a (Fig. S1A), and this Higd-1a silencing led to growth inhibition of both AsPC-1 and PANC-1 cell lines, as defined by trypan blue exclusion (Figs. S1B and C). After 4 days, cell numbers in the Higd-1a-depleted AsPC-1 and PANC-1 cultures were only 41 and 43%, respectively, of those in control shRNA-transfected cells. In MTT proliferation assays, Higd-1a silencing clearly reduced the growth of AsPC-1 cells (Fig. S1D). To see whether the growth retardation was caused by increased apoptosis or reduced proliferation we used Annexin V^-/propidium $iodide^-$ to identify viable cells. There were no signs of apoptosis in the cultures depleted of Higd-1a, as the percentages of viable cells (Annexin-V^- and PI^-) in the Higd-1a-depleted cultures were similar to those in control cultures in both cell lines (Fig. 1C). To further define the mechanism of growth retardation, we analyzed cell cycle progression of AsPC-1 cells and found that Higd-1a depletion led to cell cycle retardation in the G1 phase. The G1 phase of the Higd-1a-depleted AsPC-1 cells increased from 54.7 ± 0.7% to 65.0 ± 0.8% with a corresponding decrease in the proportion of cells in the S and G2 phases after 6 days (Fig. 1D). In PANC-1 cells, the G1 phase was similarly

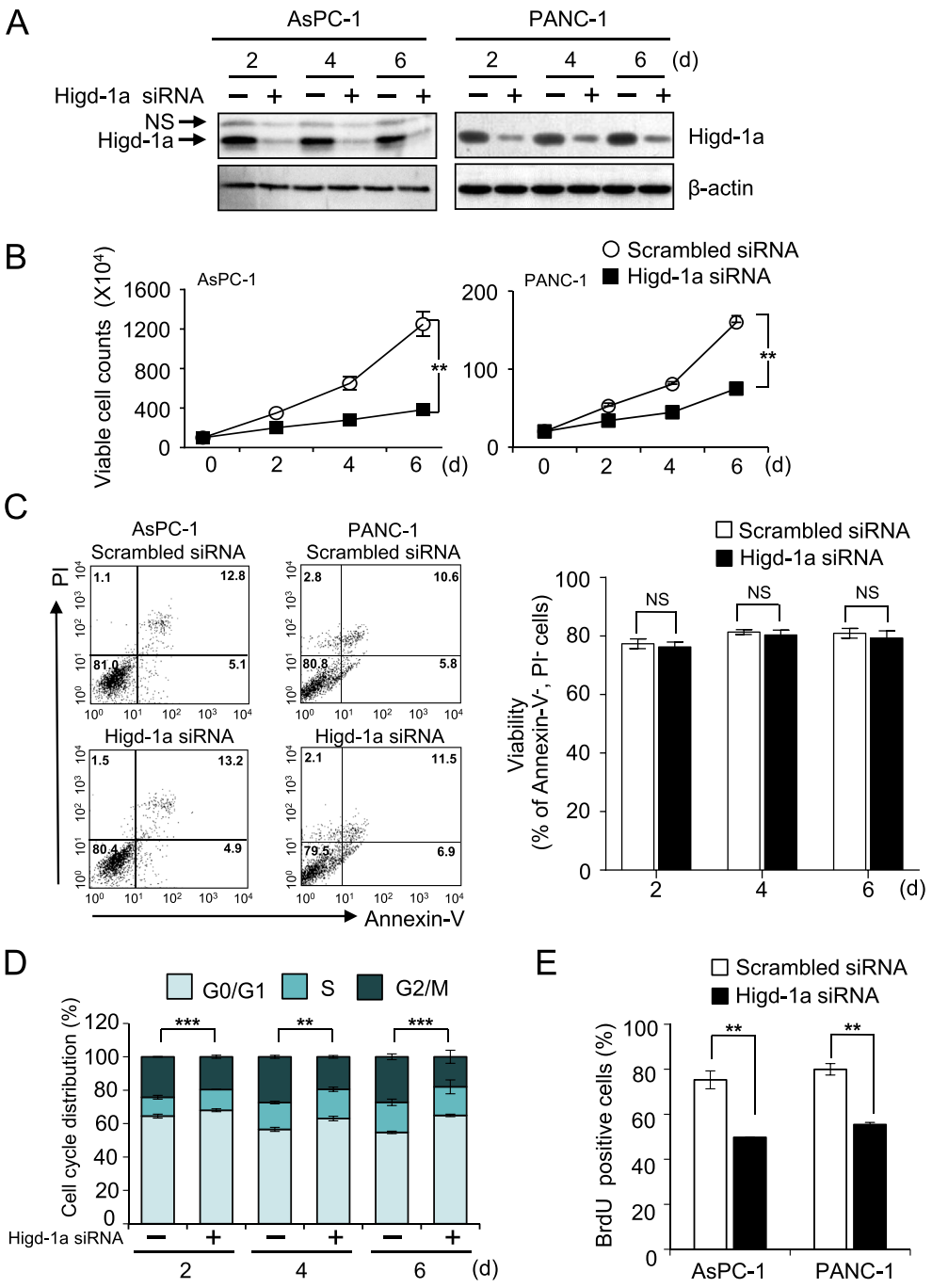

Fig. 1. Silencing of Higd-1a expression inhibits cell proliferation. (A-B) AsPC-1 and PANC-1 cells were transiently transfected with scrambled (−) or Higd-1a (+) siRNA. Total cell extracts were immunoblotted with anti-Higd-1a polyclonal antibody at the indicated times after transfection. β-actin was used as a loading control (A). Total viable cells were counted by trypan blue exclusion (B). (C) Annexin V/propidium iodide staining was performed 4 days after siRNA transfection (left). Percentages of annexin V and propidium iodide negative cells (viable cells) of AsPC-1 cells were quantified by flow cytometry at the indicated times after transfection (right). (D) AsPC-1 cells were stained with propidium iodide and were examined by flow cytometric cell cycle analysis after transient transfection with siRNA. Cell cycle distributions were analyzed with ModFit LT software. (E) Cells were pulse-labeled with 50 μM BrdU for 24 h after 3 days of siRNA transfection and were stained with an anti-BrdU antibody. Measurements were performed by flow cytometry. Results shown are representative of three independent experiments. Data are means ± S.E., **; $p < 0.01$, ***; $p < 0.001$. (For interpretation of the references to color in this figure legend, the reader is referred to the Web version of this article.)

increased by Higd-1a silencing (from 54.0 ± 2.8% to 67.4 ± 1.5%, Fig. S2A). Furthermore, bromodeoxyuridine incorporation into the DNA of actively proliferating cells fell by about 30% after pulse labeling for 24 h after 4 days of higd-1a depletion in both cell lines (Fig. 1E). Collectively, our observations demonstrate that Higd-1a silencing leads to growth retardation of cancer cells without inducing cell death.

3.2. Higd-1a depletion induces a senescence phenotype

Careful observation showed that Higd-1a depletion also increased the number of flattened and enlarged cells (Fig. 2A). Since senescence involves essentially irreversible growth arrest, enhanced size and granularity, we investigated whether depletion of Higd-1a induced senescence. Flow cytometry analysis showed that depletion of Higd-1a increased cellular granularity in addition to cell size (1.5-fold in AsPC-1 and 2.1-fold in PANC-1) (Fig. 2B). We also measured SA-β-gal activity, a specific marker of senescence. There was a more than 3-fold increase of SA-β-gal activity in Higd-1a-depleted AsPC-1 and PANC-1 cells (Fig. 2C). Based on these results, we conclude that inhibition of Higd-1a induces the major features of cell senescence in pancreatic cancer cells.

Senescent cells often secrete proinflammatory cytokines, chemokines, growth factors and proteases that bring about immune clearance of the cells [21]. This senescence-associated secretory phenotype (SASP) is usually regulated by IL-1- and NF-κB-driven pathways. In Higd-1a-silenced ASPC-1 cells, however, of the factors involved in SASP, MMP1, MMP2, MMP3, CXCL1, CCL20 and IL-1β were not significantly changed (Fig. 2D) though TNF-α and IL-8 did increase (1.4, and 2.7 fold, respectively). The levels of most of the cytokines and chemokines, including IL-8, were also not significantly altered in the Higd-1a-silenced PANC-1 cells, except for MMP3 and CCL20, which

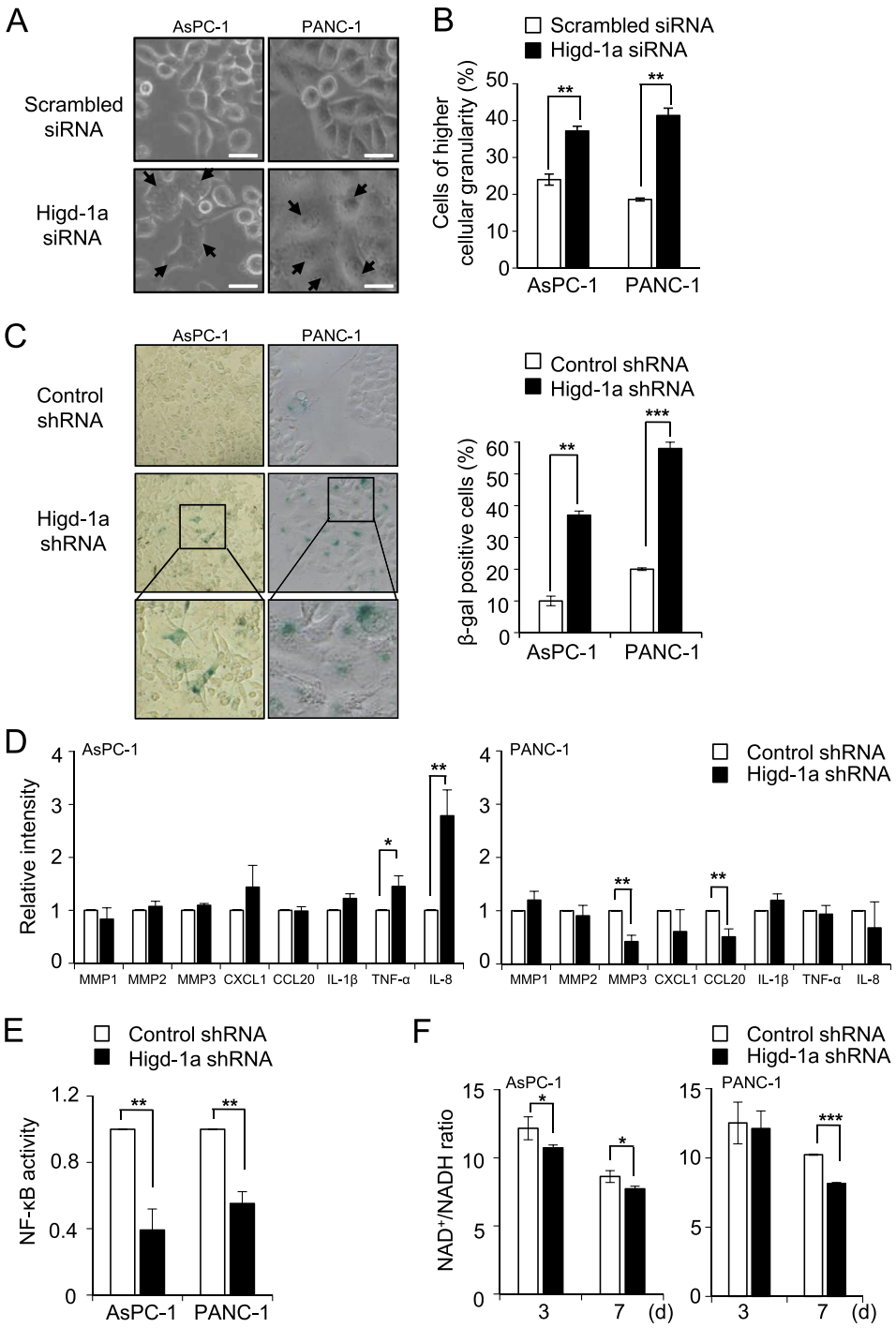

Fig. 2. Higd-1a depletion induces senescence. (A) Cell morphologies were observed by conventional light microscopy, and photographs of representative shapes are shown. Bar; 30 μM. (B) Flow cytometric analysis of the granularity of control and Higd-1a-depleted cells. Cells were acquired and analyzed by SSC *vs.* FSC. Percentages of higher cellular granularity were obtained from the upper portion of gates indicating higher SSC level. (C) Cells were infected with lentiviruses expressing control or Higd-1a shRNA. Twelve days after infection, they were fixed and incubated in freshly prepared β-galactosidase staining solution. The stained cells were observed under an inverted microscope (left). Senescence-associated β-galactosidase-positive cells were counted among 300 cells chosen at random (right). Data represent means ± S.E. of three independent experiments. (D) AsPC-1 and PANC-1 cells were infected with lentiviruses expressing control or Higd-1a shRNA. After 12 days, cells were harvested and semi-quantitative RT-PCR was performed to measure the expression of the indicated cytokines and chemokines. (E-F) Seven days after infection with the shRNA lentivirus, cells were harvested to measure the NF-κB activity levels (E) and NAD+/NADH ratios (F). *; $p < 0.05$, **; $p < 0.01$, ***; $p < 0.001$.

decreased by 57% and 50%, respectively. Furthermore, NF-κB activity was reduced in both sets of Higd-1a-silenced cells (Fig. 2E). Therefore, SASP may not be responsible for cellular senescence in Higd-1a-silenced pancreatic cancer cells. Recently, Wiley et al. reported that senescence induced by mitochondrial damage represents a unique phenotype due to a reduced NAD+/NADH ratio and independent of IL-1-dependent SASP and NF-κB activities [22]. In the Higd-1a knockdown cells, the NAD+/NADH ratios was indeed consistently lower than in the control cells (Fig. 2F). Therefore, we conclude that Higd-1a depletion induces a senescence phenotype that is specifically associated with mitochondrial dysfunction.

3.3. Higd-1a depletion retards the growth of cancer cells in xenografted nude mice

Based on the growth retardation and senescence phenotype found in Higd-1a-depleted cells, we subsequently sought to determine whether Higd-1a silencing affected the growth of AsPC-1 and PANC-1 tumors in xenografted nude mice. Cancer cells were infected with Higd-1a or scrambled shRNA, selected with puromycin for 3 days, and injected into nude mice. Higd-1a depletion inhibited the growth of AsPC-1 tumors by as much as 72% by volume after 21 days (Fig. 3A), after which the tumors were removed from the animals and weighed. The average weight of the tumors from the Higd-1a knockdown mice was 85% lower than that for the tumors from the control group. Knockdown of Higd-1a

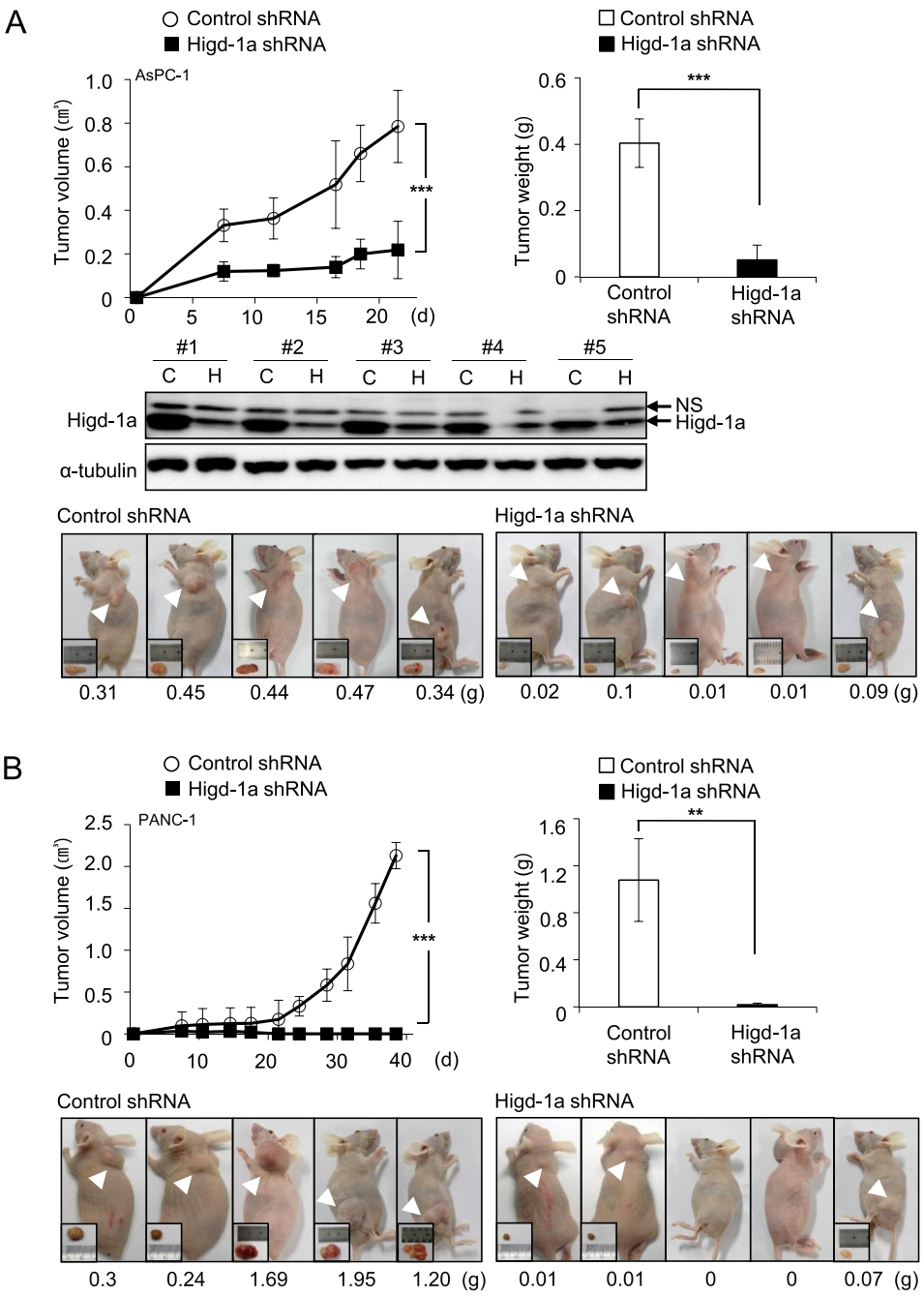

Fig. 3. Silencing of Higd-1a expression inhibits cancer cell growth in xenografted nude mice. Three days after infection with the control or Higd-1a shRNA lentivirus, AsPC-1 or PANC-1 cells were screened with puromycin for 3 days. Five nude mice per group were injected subcutaneously with 1×10^6 cells each. (A) AsPC-1 tumor volumes were measured for up to 21 days (left). At 21 days, the mice were killed to measure the tumor weights (right) and for the immunostaining of Higd-1a (middle). C; Control shRNA, H; Higd-1a shRNA. Representative mice bearing xenografts of control versus Higd-1a knockdown cells are shown in the bottom panel. (B) PANC-1 tumor volumes were measured for up to 38 days (left) and the tumors weighed (right). Representative mice bearing xenografts of control versus Higd-1a knockdown cells are shown in the bottom panel. **; $p < 0.01$, ***; $p < 0.001$.

in the tumors was verified by Immunoblotting (Fig. 3A, middle panel). Higd-1a-silenced PANC-1 cells failed to form tumor masses and their growth was inhibited by around 99% by weight after 38 days (Fig. 3B).

3.4. *Higd-1a depletion induces cell cycle arrest of pancreatic cancer cells through $p27^{KIP1}$/pRB*

We have shown above that Higd-1a depletion inhibits cancer cell growth *in vitro* and in xenografted mice (Figs. 1 and 3) and that this is not due to stimulating apoptosis (Fig. 1C), but to inhibition of proliferation (Fig. 1D and E).

To understand the mechanism underlying the cell cycle retardation in Higd-1a knockdown cells, we first measured the mRNAs for genes that control the G0/G1 checkpoint in AsPC-1 cells. Of the INK and CIP/KIP cell cycle inhibitors, $p27^{KIP1}$ was significantly up-regulated by depletion of Higd-1a 6 days after knockdown of Higd-1a, and $p16^{INK4a}$, $p19^{ARF}$ and $p21^{CIP1}$ were not induced (Fig. 4A). Although $p16^{INK4a}$ was induced at later times, this may not represent functional protein since the gene is known to be disrupted by a frame-shift mutation in AsPC-1 cells [23]. Both cyclins D1 and E were reduced after 12 days. Paralleling the mRNA changes, $p27^{KIP1}$ protein increased significantly and cyclins D1 and E declined slightly in AsPC-1 cells (Fig. 4B). Phosphorylation of RB protein lies downstream of $p27^{KIP1}$, cyclin D1 and cyclin E [24], and RB phosphorylation was clearly reduced in the Higd-1a-depleted cells. In a time-dependent manner, $p27^{KIP1}$ protein expression starts to be induced after 3 days of Higd-1a depletion, lasting for up to 6 days (Fig. 5A). In PANC-1 cells, the increase of the $p27^{KIP1}$ protein was also prominently caused by Higd-1a silencing, and cyclin D1 and RB phosphorylation levels were decreased, although there was no change in the cyclin E expression level (Fig. S2B). To investigate the role of $p27^{KIP1}$ in the cell cycle arrest, Higd-1a knockdown cells were transfected with $p27^{KIP1}$ siRNA. The amount of p27 induced was efficiently

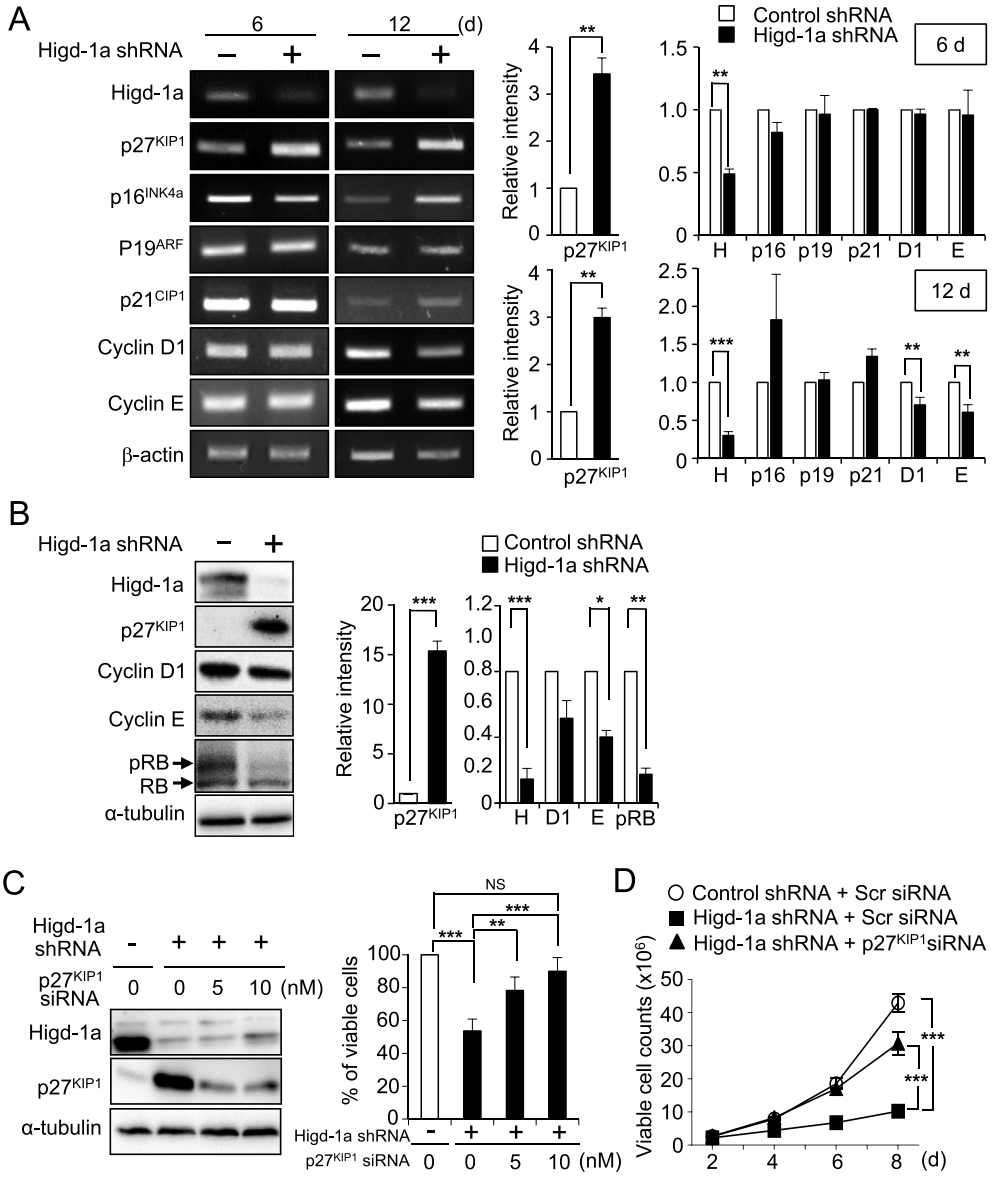

Fig. 4. Silencing of Higd-1a expression induces cell cycle arrest by inducing p27^{KIP1}. (A) RT-PCR analyses of various cell cycle regulatory genes in AsPC-1 cells at the indicated times after infection with control or Higd-1a shRNA (left). The relative intensities of the PCR bands were analyzed with ImageJ (right). Data are representative of three independent experiments. (B) Total cellular proteins were extracted 6 days after infection with the shRNA virus and the levels of the indicated proteins were determined by immunoblot analysis. α-tubulin was used as a loading control (left). The relative intensities of the immunoblot bands were analyzed with ImageJ, normalized according to the α-tubulin expression level, and are expressed as percentages relative to cells infected with control shRNA (right). (C) AsPC-1 cells were infected with the control or Higd-1a shRNA virus and transiently transfected with scrambled or p27^{KIP1} siRNA at the indicated concentrations after 24 h. Four days after infection, the levels of the indicated proteins were determined by immunoblot analysis (left), and total viable cells were counted by trypan blue exclusion and expressed as percentages relative to control cells (right). (D) AsPC-1 cells were infected with the control or Higd-1a shRNA and transfected with 10 nM scrambled or p27^{KIP1} siRNA, as in (C). Total viable cells were counted at the indicated time points. Data are means ± S.E. of three independent experiments. *; $p < 0.05$, **; $p < 0.01$, ***; $p < 0.001$.

reduced by the siRNA (Fig. 4C, left). Growth of the Higd-1a-p27^{KIP1} double knockdown cells reached almost 90% of that of the control AsPC-1 cells after 4 days of infection, while growth of the Higd-1a single knockdown cells was again strongly inhibited (Fig. 4C, right). The recovery of cell growth by p27^{KIP1} depletion is clearly shown in a time-dependent manner up to 8 days of Higd-1a depletion in Fig. 4D. Taken together, these observations suggest that the growth retardation resulting from Higd-1a depletion is a consequence of the differential expression of cell cycle regulatory proteins, especially p27^{KIP1}, and involves cell cycle arrest in G1 phase.

3.5. Higd-1a expression regulates the ERK signaling pathway

Next, we investigated the upstream signaling pathways regulating expression of p27 ^{KIP1}. In Higd-1a-depleted AsPC-1 cells, phosphorylation of ERK was reduced by > 50% in repeated experiments (Figs. S3A and B), while phosphorylation of the other MAP kinases, p38MAPK and JNK, was unchanged. Activation of the AKT/mTor/S6K pathway and phosphorylation of AMPK were not induced, and the expression of GSK-3β was also unaffected. In Higd-1a-depleted PANC-1 cells, reduced ERK phosphorylation was similarly repeated, as in AsPC-1 cells (Figs. S3C and D). To check the down-regulation of p-ERK1/2 clearly, we detected p-ERK1/2 levels as a function of time after the knockdown of Higd-1a in AsPC-1 cells. p-ERK1/2 was reduced by day 3 and continued to decrease up to day 6 (Fig. 5A). We examined whether the ERK pathway is regulated downstream of Higd-1a, by means of Higd-1a reconstitution. Higd-1a-Flag overexpression by transient transfection led to high expression of the fusion protein and was clearly detected by Flag antibody immunoblotting (Fig. 5B). Because Higd-1a depletion was performed by Higd-1a shRNA, the endogenous Higd-1a expression was also restored slightly by Higd-1a-Flag overexpression. The relatively less-regulated pERK phosphorylation process was clearly recovered by the reconstitution of Higd-1a in a time-dependent manner, and the growth of Higd-1a-Flag transfected cells reached nearly 85% of that of the control AsPC-1 cells, whereas the rate of Higd-1a-depleted cells was only 33% after 5 days. We also assessed whether the reduced activation of the ERK pathway had a direct effect on p27^{KIP1} induction and cell cycle arrest. AsPC-1 cells were treated with U0126 and SB203580, which are inhibitors of MEK and p38MAPK, respectively. U0126 treatment completely inhibited phosphorylation of ERK1/2 and concomitantly induced expression of p27^{KIP1} (Fig. 5C). SB203580 did not have any significant effect on the phosphorylation of ERK1/2 and did not enhance the expression of p27^{KIP1}. These results indicated that cell cycle arrest caused by Higd-1a depletion is controlled by the down-regulation

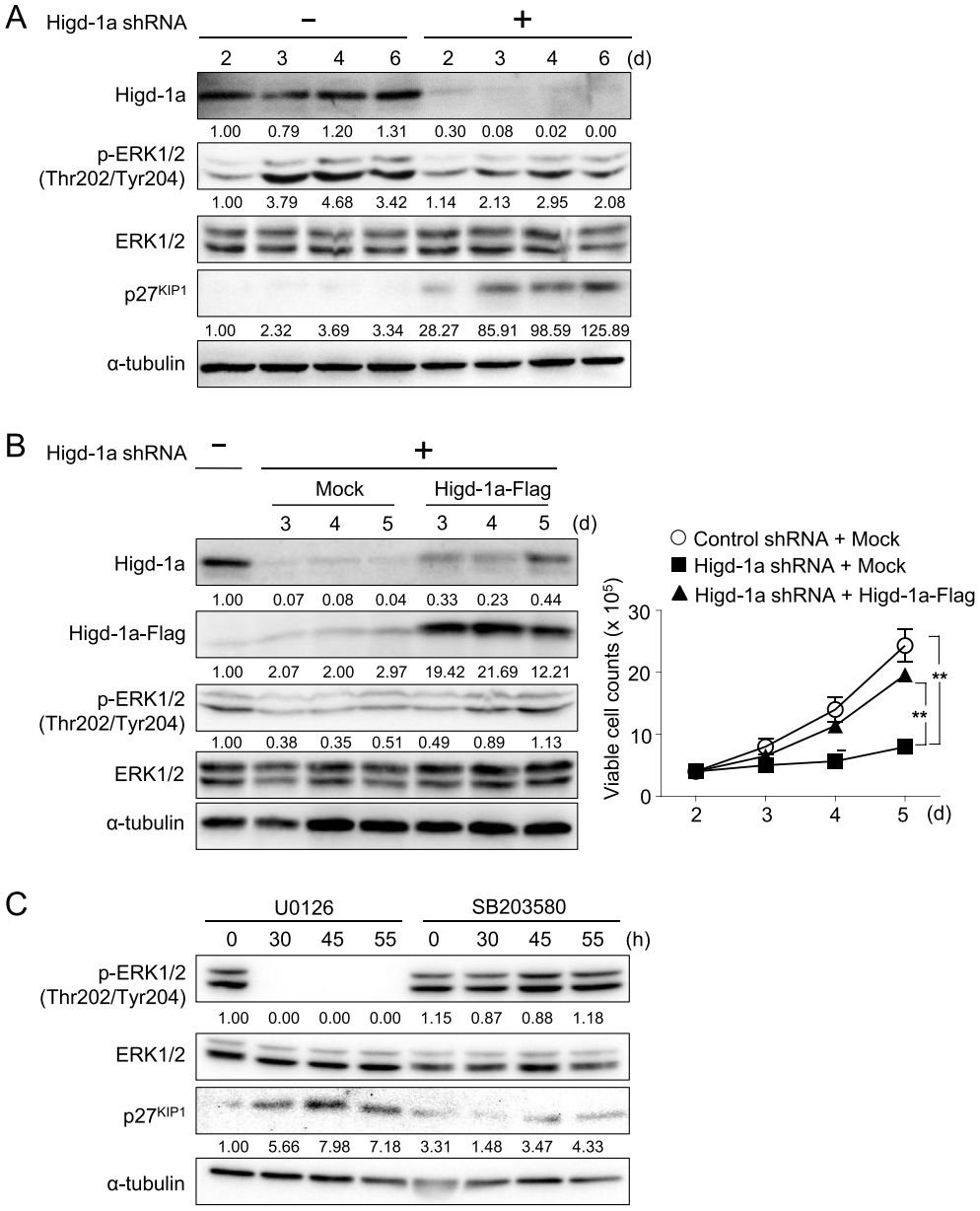

Fig. 5. Silencing of Higd-1a expression inhibits ERK phosphorylation. (A) AsPC-1 cells were infected with lentivirus expressing control or Higd-1a shRNA. The levels of Higd-1a, phosphorylated ERK, total ERK and $p27^{KIP1}$ protein were determined by immunoblotting at the indicated times after transfection. (B) AsPC-1 cells were infected with lentivirus expressing control or Higd-1a shRNA. After 24 h, cells were transfected with the Higd-1a-Flag plasmid. The expression levels of the indicated proteins were determined by immunoblotting at the indicated times after transfection (left) and the total viable cells were counted at the indicated time points (right). (C) AsPC-1 cells were treated with 10 μM U0126 (an MEK inhibitor) and 2 μM SB203580 (a p38MAPK inhibitor). Total cell lysates were analyzed for phosphorylated ERK, total ERK and $p27^{KIP1}$ expression by immunoblotting. Relative intensities were analyzed using ImageJ, normalized by α-tubulin expression, and are shown as numbers. Data are representative of three independent experiments.

of the ERK pathway and the induction of $p27^{KIP1}$ in pancreatic cancer cells.

3.6. Higd-1a expression is up-regulated in human pancreatic cancers

Next, we analyzed two GEO transcriptome microarray datasets (36 human pancreatic tumor tissues and 16 normal tissues in GDS4102; 45 pancreatic ductal adenocarcinoma tumor tissue and 45 adjacent non-tumor tissues in GDS4336), to examine the expression level of Higd-1a mRNA in tumor tissue. In both datasets, Higd-1a expression was significantly elevated in pancreatic tumor tissue ($P = 0.0045$ and 0.00022, respectively) (Fig. 6A), suggesting that enhanced expression of Higd-1a is associated with pancreatic tumorigenesis. Of other proteins involved in mitochondrial fusion and fission, only DRP1 was significantly elevated in pancreatic cancers (Fig. S4); OPA1, MFN1 and MFN2 were not significantly affected. DRP1 is known to be induced in several other cancers, such as breast carcinoma, lung cancer and glioblastoma [25–27]. These results provide clinical evidence for a survival role of Higd-1a in pancreatic cancer.

To explore the relationship between Higd-1a and cell cycle regulation in pancreatic cancer, we examined the correlation between Higd-1a mRNA levels and cell cycle regulators, using the GDS4336 dataset. As shown in Fig. 6B, expression of Higd-1a was positively correlated with that of CCNA2 (cyclin A), CCNE2 (cyclin E), CDK1 and CDK2, and negatively correlated with that of $p27^{KIP1}$ and $p57^{KIP2}$. These data are consistent with the *in vitro* findings in Fig. 3, showing induced $p27^{KIP1}$ expression and reduced cyclin E expression as a result of silencing of Higd-1a. Furthermore, Higd-1a expression was positively related with that of the E2F target genes, PCNA, DHFR and CDK1 (Fig. 6B), consistent with the data in Fig. 3B indicating down-regulation of RB phosphorylation, the major regulator of the E2F transcription factor. To confirm this bioinformatics analysis, we analyzed the expression of E2F target genes in Higd-1a-depleted AsPC-1 and PANC-1 cells using semi-quantitative RT-PCR. Expression of the E2F target genes PCNA, DHFR, CDK1 and TK1 was reduced by depletion of Higd-1a in both cell lines (Fig. 6C and Fig. S2C). These results provide clinical evidence that the survival role of Higd-1a in pancreatic cancer cells is closely related to the control of cell cycle regulatory factors.

Finally, immunohistochemistry was performed to examine the protein expression levels of Higd-1a in pancreatic tissues of human

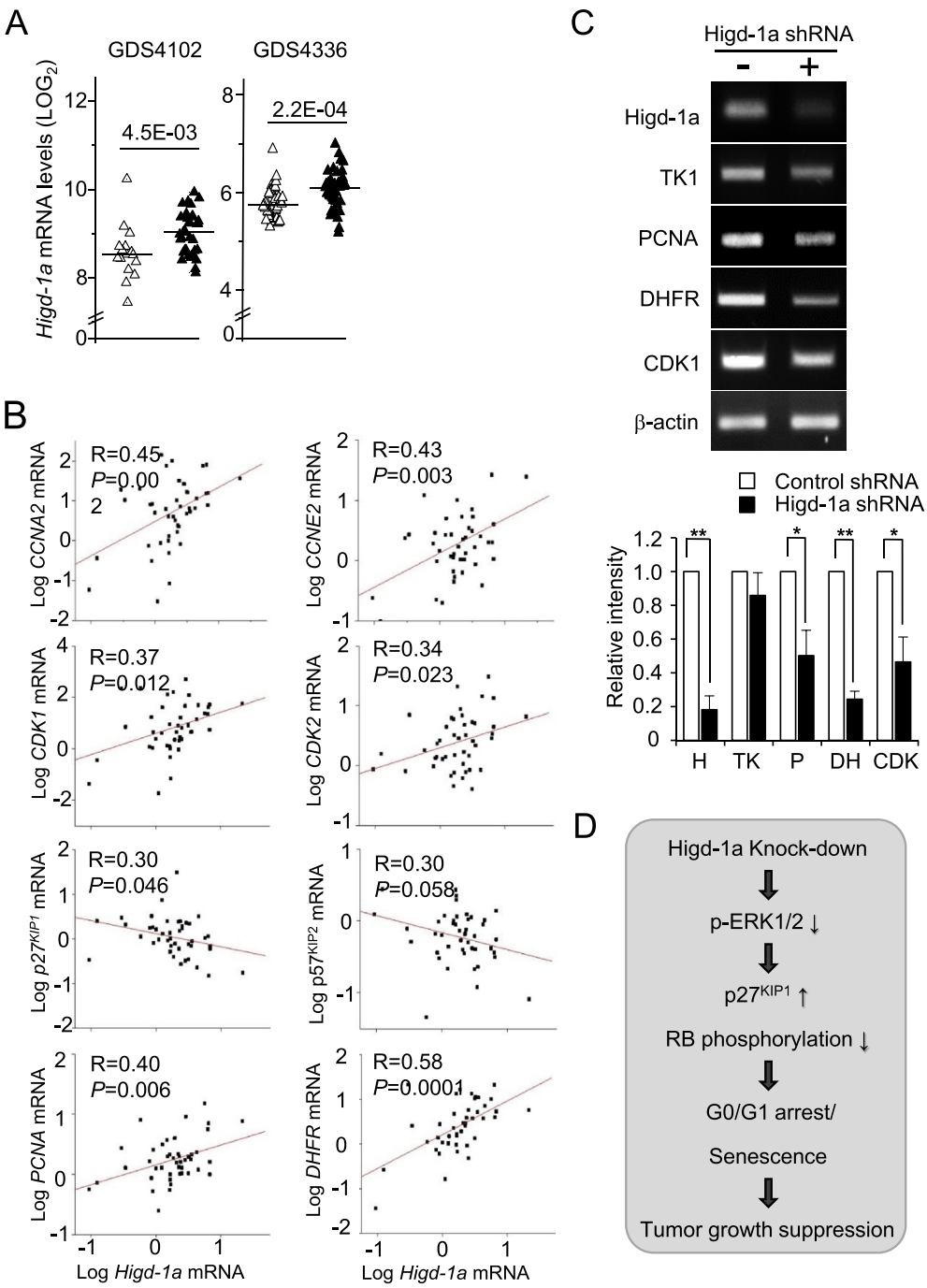

Fig. 6. Higd-1a mRNA expression is up-regulated in human pancreatic cancer tissues. (A) Higd-1a mRNA expression was analyzed in two different gene sets of pancreatic tumors. The GDS4102 data set contains 52 samples (36 pancreatic tumors and 16 normal tissue samples), and the GDS4336 data set contains 90 samples (45 pancreatic ductal adenocarcinomas and 45 adjacent non-tumor tissue samples). Differences were analyzed using Student's *t*-test. (B) Scatter plots of the $\log_2$ values of Higd-1a mRNA expression versus that of cell cycle related genes (CCNA2, CCNE2, CDK2, $p27^{KIP1}$, $p57^{KIP2}$) and E2F target genes (PCNA, DHFR, CDK1) in the 45 pancreatic tumor tissues in the GDS4336 data set. R; gradient. P; significance value. (C) mRNA levels of E2F target genes in AsPC-1 cells after 12 days of lentiviral infection with control or Higd-1a shRNA (upper). The relative intensities of the PCR bands were analyzed with ImageJ (bottom). Higd-1a (H), TK1 (TK), PCNA (P), DHFR (DH), CDK1 (CDK). Data are representative of three independent experiments. (D) Schematic representation of the proposed mechanism underlying the cell cycle retardation and senescence induced by Higd-1a depletion.

patients. Twelve each of paraffin-embedded pancreatic cancer tissues and adjacent non-cancer tissues were adopted. As shown in Fig. 7, Higd-1a expression levels were found to be highly elevated in pancreatic cancer tissues. The increased mean Higd-1a staining scores in pancreatic cancer tissues was markedly significant compared to adjacent non-cancer tissues (p = 0.00001). Nuclear Ki-67 was used as a cellular marker for the proliferation of cancer tissues. The average of Ki-67 positive cells showed a 20-fold increase in pancreatic cancer tissues (p = 0.0000029). Collectively, these results indicate that enhanced Higd-1a protein expression levels are highly correlated with pancreatic cancerous progression.

4. Discussion

In this study, we characterized the role of Higd-1a in the proliferation of pancreatic cancer cells and concluded that depletion of Higd-1a leads to inhibition of tumor growth by the mechanism outlined in Fig. 6D. This schema is based on several observations. First, Higd-1a depletion inhibited cancer cell growth *in vitro* and in mouse xenografts. (Figs. 1 and 3). Second, this growth retardation did not result from apoptosis but from cell cycle retardation through induction of $p27^{KIP1}$ and RB hypo-phosphorylation (Figs. 1 and 4 and Fig. S2B). Third, Higd-1a knockdown reduced ERK phosphorylation and this is likely to be responsible for the induction of $p27^{KIP1}$ since U0126, which inhibits ERK phosphorylation, mimicked the effect of Higd-1a depletion (Fig. 5). Fourth, Higd-1a-depleted cells were mainly retarded in G0/G1 and displayed the characteristics of senescence (Fig. 2). Fifth, Higd-1a expression was up-regulated in pancreatic cancer tissue, and its level of expression was consistently correlated with that of cell cycle regulatory genes (Figs. 6 and 7).

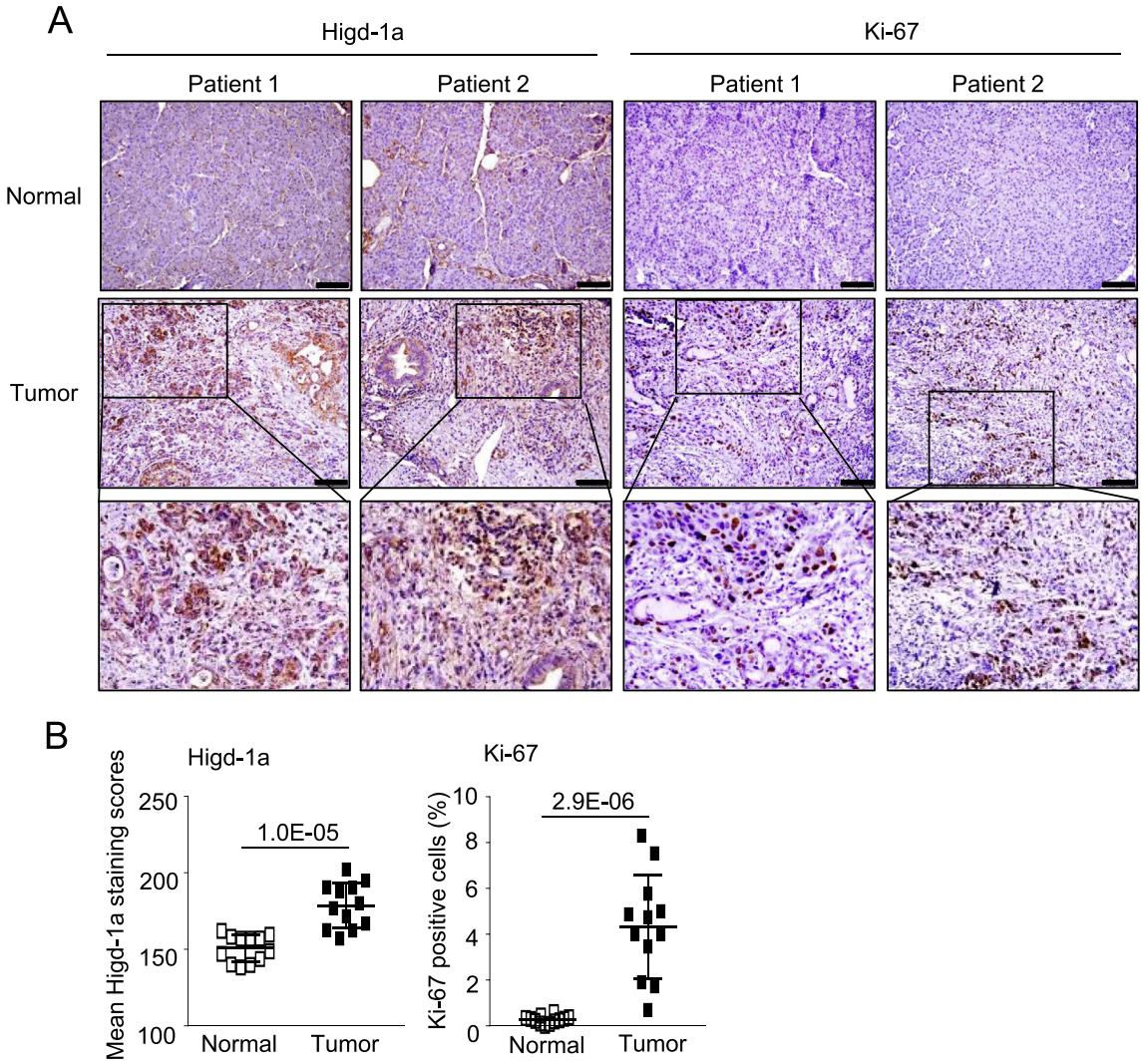

Fig. 7. Higd-1a protein expression is upregulated in human pancreatic cancer tissues. (A) Immunohistochemistry (IHC) staining for Higd-1a and Ki-67 protein expression in 12 each of paraffin-embedded pancreatic cancer and adjacent non-tumor (normal) tissues (X200). Typical examples among tissue IHC outcomes are shown. Bar; 100 μM. (B) Statistical analysis of the mean Higd-1a staining scores and Ki-67 positive cells between pancreatic cancer and corresponding non-tumor tissues. Differences were analyzed using multiple t tests.

Cell cycle progression is often affected in human cancers. The cell cycle is driven forward by cyclin-dependent kinases (CDKs), and members of the KIP/CIP family of CDK inhibitors, $p21^{CIP1}$, $p27^{KIP1}$, and $p57^{KIP2}$, negatively regulate CDK activity at the G1/S phase transition [28]. It has been reported that the RAS/RAF/MAPK and PI3K/AKT pathways, commonly mutated in human cancer, can directly influence the expression and activity of $p27^{KIP1}$ [28]. Interestingly, in our screen of kinase pathways by immunoblotting, only ERK activation was reduced during $p27^{KIP1}$ induction, with no change in kinases such as JNK, p38, GSK-3β, AMPK, and kinases of the AKT/mTor pathway. There have been many studies of the regulation of $p27^{KIP1}$ expression by the ERK pathway. When ERK1/2 is phosphorylated in response to a mitogen, Skp2, an F-box protein of the E3 ubiquitin ligase complex, increases and $p27^{KIP1}$ protein declines due to ubiquitination. Increased ERK activation also inhibits the expression of the transcription factor FOXO3, and this further reduces expression of $p27^{KIP1}$ [24,29–31]. We also observed that $p27^{KIP1}$ increased in response to the ERK1/2 phosphorylation inhibitor U0126, confirming that $p27^{KIP1}$ is regulated via the ERK pathway (Fig. 5B).

Senescence is a state of irreversible growth arrest in G0/G1 phase due to loss of responsiveness to growth factors. It is mainly generated via the p53 and RB pathways [32]. The cyclin-dependent kinase inhibitors, $p16^{INK4a}$ and $p21^{CIP1}$, are regarded as key effectors of cellular senescence. $p16^{INK4a}$ inhibits CDK4/6, which leads to RB hypophosphorylation, and its upregulation is essential in the terminal stages of growth arrest in senescence [3,33]. $p21^{CIP1}$ is an inhibitor of CDK2 and a p53 target for the induction of senescence. However, the AsPC-1 pancreatic cancer cells used in our experiments harbor a $p16^{INK4a}$ frameshift and a TP53-inactivating mutation [23], which is consistent with the finding that *KRAS* [> 90%], $p16^{INK4A}$ [> 90%] and *TP53* [> 70%] are hallmark mutations of human pancreatic adenocarcinomas [34]. Interestingly, therefore, Higd-1a depletion of AsPC-1 cells induced $p27^{KIP1}$ expression and led to growth retardation and senescence in the absence of $p16^{INK4a}$ and TP53. There have been several reports linking senescence and $p27^{KIP1}$ induction. In U20S osteosarcoma cells, which have mutations in TP53 and the RB locus, reintroduction of RB or ectopic expression of $p27^{KIP1}$ induced senescence [35]. In prostatic intraepithelial neoplasias that did not develop to invasive cancer, $p27^{KIP1}$ knock-out inhibited senescence and led to the development of invasive cancer [3]. Senescence induced by loss of the von Hippel-Lindau tumor suppressor (VHL) in renal cancer cells is RB-, $p27^{KIP1}$- and Skp2-dependent but p53-independent [36]. Furthermore, Inhibition of the PI3K pathway in normal mouse embryonic fibroblasts (MEF) cells leads to senescence that is associated with increased levels

of $p27^{KIP1}$, but not of TP53, $p19^{ARF}$, $p16^{INK4a}$, or $p21^{CIP1}$ [37]. Our results are additional evidence that $p27^{KIP1}$/RB is part of an important pathway for inducing senescence in the absence of TP53 and $p16^{INK4a}$ activities.

Recently, Ameri et al. reported that in conditions of cellular stress, such as glucose deprivation, the ectopic expression of Higd-1a suppressed cell growth but strongly promoted tumor cell survival by reducing cell death by modulating oxygen consumption, ROS production and AMPK activity in HIF-1α-deficient MEF [20]. They explained that Higd-1a serves as an oncogene in severe tumor environments, although it may also act as a tumor suppresser in less severe forms of metabolic stress. We previously reported that RAW264.7 macrophages stably transfected with Higd-1a underwent less apoptosis in hypoxic conditions due to the inhibition of the release of cytochrome *c* and the reduction of caspase activities. Vice versa, hypoxia-induced apoptosis increased when endogenous Higd-1a was silenced [16]. Based on these results, Higd-1a is clearly involved in cell survival, although the level of this involvement may change depending on the cell and stress types. In the present study, we demonstrated the requirement of Higd-1a for the optimal proliferation of pancreatic cancer cells through regulation of the pERK/$p27^{KIP1}$/RB pathway. In addition, we clearly showed that both mRNA and protein expression levels of Higd-1a increase in human pancreatic cancer tissues. Mitochondria are essential for malignant tumor progression, and cancer treatments targeted at mitochondria have been found to be effective [1]. For example, metformin, an inhibitor of electron transport chain complex 1, is in clinical trials for various cancers [38]. Further studies of the role of Higd-1a in mitochondrial homeostasis and of its downstream pathways regulating intracellular signaling, may provide opportunities for the development of novel cancer treatments.

Authorship contribution statement

Conception and design: H-J. An, H. Lee, Development of methodology: H-J. An, M. Ryu, H-M. Jeon. Analysis and interpretation of data: H-J. An, M. Ryu, M. Kang, H.J. Jeong, Writing, review, and/or revision of the manuscript: J-O. Lee, Y.S. Kim and H. Lee, Administrative, technical, or material support: J-O. Lee, H. Lee, Study supervision: Y.S. Kim, H. Lee.

Conflicts of interest

The authors declare no conflicts of interest.

Acknowledgements

This research was supported by the National Research Foundation of Korea (NRF), South Korea (2013R1A1A2063431 and 2017M3A9F6029753). Human pancreatic cancer tissues were obtained from the Daegu Dongsan Hospital Biobank (Keimyung University, Daegu, Korea).

Appendix A. Supplementary data

Supplementary data to this article can be found online at https://doi.org/10.1016/j.canlet.2019.07.007.

References

[1] W.X. Zong, J.D. Rabinowitz, E. White, Mitochondria and cancer, Mol. Cell 61 (2016) 667–676.
[2] S. Vyas, E. Zaganjor, M.C. Haigis, Mitochondria and cancer, Cell 166 (2016) 555–566.
[3] D.A. Alcorta, Y. Xiong, D. Phelps, G. Hannon, D. Beach, J.C. Barrett, Involvement of the cyclin-dependent kinase inhibitor p16 (INK4a) in replicative senescence of normal human fibroblasts, Proc. Natl. Acad. Sci. U. S. A. 93 (1996) 13742–13747.
[4] F. Weinberg, R. Hamanaka, W.W. Wheaton, S. Weinberg, J. Joseph, M. Lopez, B. Kalyanaraman, G.M. Mutlu, G.R. Budinger, N.S. Chandel, Mitochondrial metabolism and ROS generation are essential for Kras-mediated tumorigenicity, Proc. Natl. Acad. Sci. U. S. A. 107 (2010) 8788–8793.
[5] A.S. Tan, J.W. Baty, L.F. Dong, A. Bezawork-Geleta, B. Endaya, J. Goodwin, M. Bajzikova, J. Kovarova, M. Peterka, B. Yan, E.A. Pesdar, M. Sobol, A. Filimonenko, S. Stuart, M. Vondrusova, K. Kluckova, K. Sachaphibulkij, J. Rohlena, P. Hozak, J. Truksa, D. Eccles, L.M. Haupt, L.R. Griffiths, J. Neuzil, M.V. Berridge, Mitochondrial genome acquisition restores respiratory function and tumorigenic potential of cancer cells without mitochondrial DNA, Cell Metabol. 21 (2015) 81–94.
[6] R.J. DeBerardinis, N.S. Chandel, Fundamentals of cancer metabolism, Sci Adv 2 (2016) e1600200.
[7] H.M. Ni, J.A. Williams, W.X. Ding, Mitochondrial dynamics and mitochondrial quality control, Redox Biol 4 (2015) 6–13.
[8] C. Frezza, S. Cipolat, O. Martins de Brito, M. Micaroni, G.V. Beznoussenko, T. Rudka, D. Bartoli, R.S. Polishuck, N.N. Danial, B. De Strooper, L. Scorrano, OPA1 controls apoptotic cristae remodeling independently from mitochondrial fusion, Cell 126 (2006) 177–189.
[9] A. Santel, M.T. Fuller, Control of mitochondrial morphology by a human mitofusin, J. Cell Sci. 114 (2001) 867–874.
[10] E. Smirnova, L. Griparic, D.L. Shurland, A.M. van der Bliek, Dynamin-related protein Drp1 is required for mitochondrial division in mammalian cells, Mol. Biol. Cell 12 (2001) 2245–2256.
[11] Y. Yoon, E.W. Krueger, B.J. Oswald, M.A. McNiven, The mitochondrial protein hFis1 regulates mitochondrial fission in mammalian cells through an interaction with the dynamin-like protein DLP1, Mol. Cell. Biol. 23 (2003) 5409–5420.
[12] S. Ehses, I. Raschke, G. Mancuso, A. Bernacchia, S. Geimer, D. Tondera, J.C. Martinou, B. Westermann, E.I. Rugarli, T. Langer, Regulation of OPA1 processing and mitochondrial fusion by m-AAA protease isoenzymes and OMA1, J. Cell Biol. 187 (2009) 1023–1036.
[13] J. Wang, Y. Cao, Y. Chen, Y. Chen, P. Gardner, D.F. Steiner, Pancreatic beta cells lack a low glucose and O2-inducible mitochondrial protein that augments cell survival, Proc. Natl. Acad. Sci. U. S. A. 103 (2006) 10636–10641.
[14] N. Denko, C. Schindler, A. Koong, K. Laderoute, C. Green, A. Giaccia, Epigenetic regulation of gene expression in cervical cancer cells by the tumor microenvironment, Clin. Cancer Res. 6 (2000) 480–487.
[15] X. Zhang, L. Degenstein, Y. Cao, J. Stein, K. Osei, J. Wang, beta-Cells with relative low HIMP1 overexpression levels in a transgenic mouse line enhance basal insulin production and hypoxia/hypoglycemia tolerance, PLoS One 7 (2012) e34126.
[16] H.J. An, H. Shin, S.G. Jo, Y.J. Kim, J.O. Lee, S.G. Paik, H. Lee, The survival effect of mitochondrial Higd-1a is associated with suppression of cytochrome C release and prevention of caspase activation, Biochim. Biophys. Acta 1813 (2011) 2088–2098.
[17] H. Hayashi, H. Nakagami, M. Takeichi, M. Shimamura, N. Koibuchi, E. Oiki, N. Sato, H. Koriyama, M. Mori, R. Gerardo Araujo, A. Maeda, R. Morishita, K. Tamai, Y. Kaneda, HIG1, a novel regulator of mitochondrial gamma-secretase, maintains normal mitochondrial function, FASEB J. 26 (2012) 2306–2317.
[18] H.J. An, G. Cho, J.O. Lee, S.G. Paik, Y.S. Kim, H. Lee, Higd-1a interacts with Opa1 and is required for the morphological and functional integrity of mitochondria, Proc. Natl. Acad. Sci. U. S. A. 110 (2013) 13014–13019.
[19] T. Hayashi, Y. Asano, Y. Shintani, H. Aoyama, H. Kioka, O. Tsukamoto, M. Hikita, K. Shinzawa-Itoh, K. Takafuji, S. Higo, H. Kato, S. Yamazaki, K. Matsuoka, A. Nakano, H. Asanuma, M. Asakura, T. Minamino, Y. Goto, T. Ogura, M. Kitakaze, I. Komuro, Y. Sakata, T. Tsukihara, S. Yoshikawa, S. Takashima, Higd1a is a positive regulator of cytochrome c oxidase, Proc. Natl. Acad. Sci. U. S. A. 112 (2015) 1553–1558.
[20] K. Ameri, A. Jahangiri, A.M. Rajah, K.V. Tormos, R. Nagarajan, M. Pekmezci, V. Nguyen, M.L. Wheeler, M.P. Murphy, T.A. Sanders, S.S. Jeffrey, Y. Yeghiazarians, P.F. Rinaudo, J.F. Costello, M.K. Aghi, E. Maltepe, HIGD1A regulates oxygen consumption, ROS production, and AMPK activity during glucose deprivation to modulate cell survival and tumor growth, Cell Rep. 10 (6) (2015) 891–899.
[21] J.P. Coppe, C.K. Patil, F. Rodier, Y. Sun, D.P. Munoz, J. Goldstein, P.S. Nelson, P.Y. Desprez, J. Campisi, Senescence-associated secretory phenotypes reveal cell-nonautonomous functions of oncogenic RAS and the p53 tumor suppressor, PLoS Biol. 6 (2008) 2853–2868.
[22] C.D. Wiley, M.C. Velarde, P. Lecot, S. Liu, E.A. Sarnoski, A. Freund, K. Shirakawa, H.W. Lim, S.S. Davis, A. Ramanathan, A.A. Gerencser, E. Verdin, J. Campisi, Mitochondrial dysfunction induces senescence with a distinct secretory phenotype, Cell Metabol. 23 (2016) 303–314.
[23] P.S. Moore, B. Sipos, S. Orlandini, C. Sorio, F.X. Real, N.R. Lemoine, T. Gress, C. Bassi, G. Kloppel, H. Kalthoff, H. Ungefroren, M. Lohr, A. Scarpa, Genetic profile of 22 pancreatic carcinoma cell lines. Analysis of K-ras, p53, p16 and DPC4/Smad4, Virchows Arch. 439 (2001) 798–802.
[24] S. Pramod, K. Shivakumar, Mechanisms in cardiac fibroblast growth: an obligate role for Skp2 and FOXO3a in ERK1/2 MAPK-dependent regulation of p27kip1, Am. J. Physiol. Heart Circ. Physiol. 306 (2014) H844–H855.
[25] J. Zhao, J. Zhang, M. Yu, Y. Xie, Y. Huang, D.W. Wolff, P.W. Abel, Y. Tu, Mitochondrial dynamics regulates migration and invasion of breast cancer cells, Oncogene 32 (2013) 4814–4824.
[26] J. Rehman, H.J. Zhang, P.T. Toth, Y. Zhang, G. Marsboom, Z. Hong, R. Salgia, A.N. Husain, C. Wietholt, S.L. Archer, Inhibition of mitochondrial fission prevents cell cycle progression in lung cancer, FASEB J. 26 (2012) 2175–2186.
[27] Y.Y. Wan, J.F. Zhang, Z.J. Yang, L.P. Jiang, Y.F. Wei, Q.N. Lai, J.B. Wang, H.B. Xin, X.J. Han, Involvement of Drp1 in hypoxia-induced migration of human glioblastoma U251 cells, Oncol. Rep. 32 (2014) 619–626.
[28] S.W. Blain, H.I. Scher, C. Cordon-Cardo, A. Koff, p27 as a target for cancer therapeutics, Cancer Cell 3 (2003) 111–115.

[29] K.V. Bhatt, L.S. Spofford, G. Aram, M. McMullen, K. Pumiglia, A.E. Aplin, Adhesion control of cyclin D1 and p27Kip1 levels is deregulated in melanoma cells through BRAF-MEK-ERK signaling, Oncogene 24 (2005) 3459–3471.
[30] M. Kortylewski, P.C. Heinrich, M.E. Kauffmann, M. Bohm, A. MacKiewicz, I. Behrmann, Mitogen-activated protein kinases control p27/Kip1 expression and growth of human melanoma cells, Biochem. J. 357 (2001) 297–303.
[31] T.R. Kress, T. Raabe, S.M. Feller, High Erk activity suppresses expression of the cell cycle inhibitor p27Kip1 in colorectal cancer cells, Cell Commun. Signal. 8 (2010) 1.
[32] Y. Kong, H. Cui, C. Ramkumar, H. Zhang, Regulation of senescence in cancer and aging, J Aging Res 2011 (2011) 963172.
[33] G.H. Stein, L.F. Drullinger, A. Soulard, V. Dulic, Differential roles for cyclin-dependent kinase inhibitors p21 and p16 in the mechanisms of senescence and differentiation in human fibroblasts, Mol. Cell. Biol. 19 (1999) 2109–2117.
[34] D.A. Tuveson, J.P. Neoptolemos, Understanding metastasis in pancreatic cancer: a call for new clinical approaches, Cell 148 (2012) 21–23.
[35] K. Alexander, P.W. Hinds, Requirement for p27(KIP1) in retinoblastoma protein-mediated senescence, Mol. Cell. Biol. 21 (2001) 3616–3631.
[36] A.P. Young, S. Schlisio, Y.A. Minamishima, Q. Zhang, L. Li, C. Grisanzio, S. Signoretti, W.G. Kaelin Jr., VHL loss actuates a HIF-independent senescence programme mediated by Rb and p400, Nat. Cell Biol. 10 (2008) 361–369.
[37] S. Coats, P. Whyte, M.L. Fero, S. Lacy, G. Chung, E. Randel, E. Firpo, J.M. Roberts, A new pathway for mitogen-dependent cdk2 regulation uncovered in p27(Kip1)-deficient cells, Curr. Biol. 9 (1999) 163–173.
[38] M. Pollak, Potential applications for biguanides in oncology, J. Clin. Investig. 123 (2013) 3693–3700.